doi.org/10.36721/PJPS.2026.39.12.359.1

ATI-2341 TFA promotes acquisition of epithelial-like immunophenotype in bone marrow mesenchymal stem cells and alleviates intrauterine adhesion in a rat model

Linhua Zhu[1]*, Yongfang Yue[1] and Lili Cao[2]
[1]Department of Obstetrics, Women's Hospital, Zhejiang University School of Medicine, Hangzhou, Zhejiang, 310006, China
[2]Department of Gynecology, Hangzhou Linping District Maternal & Child Health Care Hospital, Hangzhou, Zhejiang, 311113, China

Abstract: **Background**: Intrauterine adhesion (IUA) is a common complication of endometrial injury. Bone marrow mesenchymal stem cells (BMSCs) have been implicated in endometrial repair, but strategies to enhance their therapeutic efficacy remain to be optimized. The C-X-C chemokine receptor type 4 (CXCR4)/C-X-C motif chemokine ligand 12 (CXCL12) axis plays a pivotal role in BMSC homing. **Objective**: This study aimed to test the hypothesis that ATI-2341, a functionally selective allosteric regulator of CXCR4, enhances the therapeutic efficacy of BMSCs in a rat IUA model. **Methods:** After establishing the endometrial injury model, rat BMSCs were extracted and treated with ATI-2341 TFA (100 ng/mL). IUA model rats were randomly divided into model control group, BMSCs group, BMSCs+ATI-2341 TFA group, BMSCs+PBS group and Positive control group (n=10 each). Endometrial thickness was assessed by hematoxylin and eosin (HE) staining; cell proliferation by the methyl thiazolyl tetrazolium (MTT) assay; matrix metalloproteinase-9 (MMP-9)/tissue inhibitor of metalloproteinase-1 (TIMP-1) protein expression by Western blot; and cytokeratin and vimentin expression by immunohistochemistry. **Results**: ATI-2341 TFA-pre-treated BMSCs significantly increased endometrial thickness compared to untreated BMSCs ($P < 0.05$) or estrogen ($P < 0.05$). ATI-2341 TFA enhanced BMSC proliferation at 48 h ($P < 0.05$) and 72 h ($P < 0.05$). BMSCs exposed to ATI-2341 TFA or estrogen exhibited strong cytokeratin positivity and vimentin negativity. MMP-9 was downregulated ($P < 0.05$) and TIMP-1 upregulated ($P < 0.05$) in the ATI-2341 TFA group relative to controls. **Conclusion**: ATI-2341 TFA promotes acquisition of epithelial-like immunophenotype in BMSCs within the injured endometrial microenvironment and is associated with improved endometrial morphology in IUA rats. These findings provide preliminary evidence for the functional modulation of BMSCs by CXCR4-targeted therapy in endometrial repair.

Keywords: ATI-2341 TFA; BMSC; Intrauterine adhesions; Uterine

Submitted on 08-01-2026 – Revised on 28-02-2026 – Accepted on 07-03-2026 – Available online on 07-09-2026 – Published on 01-12-2026

INTRODUCTION

The uterus and endometrium are essential for female reproductive physiology and play a critical role in pregnancy (Jia *et al*., 2024; Zhao *et al*., 2023). Although the human endometrium possesses remarkable regenerative capacity, various factors, such as miscarriage, infection, and endocrine disorders, can impair its repair and regeneration (Hu *et al*., 2023). Intrauterine adhesions (IUA), a common endometrial disorder, are characterized by local fibrosis and adhesion formation within the uterine cavity, often resulting from damage to the endometrial basal layer (Qin *et al*., 2025; Song *et al*., 2021). Once the basal layer is injured, repair often leads to scar tissue formation, making functional recovery challenging (Cheng *et al*., 2025).

Bone marrow-derived mesenchymal stem cells (BMSCs) have garnered significant attention due to their multilineage differentiation potential and suitability for autologous transplantation, which minimizes immune rejection (Chen *et al*., 2025). These cells can differentiate into endometrial cells and participate in physiological endometrial regeneration (Yuan *et al*., 2022). Under pathological conditions, BMSCs migrate to injured sites and modulate inflammation, a process largely governed by chemokine signaling (Wang *et al*., 2022). Among these, stromal cell-derived factor-1 (SDF-1, also known as CXCL12) and its primary receptor, C-X-C chemokine receptor type 4 (CXCR4), play a central role in directing BMSC homing and mobilization (Gonzalez-Meljem et al., 2023; Yang *et al*., 2024). Although an alternative receptor, CXCR7 (ACKR3), has been identified, the SDF-1/CXCR4 axis remains the dominant regulator of BMSC recruitment (Ma *et al*., 2025; Park *et al*., 2024).

The local microenvironment critically influences stem cell behavior and differentiation (Zhang *et al*., 2022). Previous studies have shown that endometrial culture medium and β-estradiol can promote stem cell differentiation into endometrial epithelial cells, suggesting that the intrauterine environment is key to inducing epithelial differentiation (Kim *et al*., 2025). However, the exact composition of endometrial culture medium remains undefined and the mechanisms underlying BMSC differentiation into

**Corresponding author:* e-mail: nickzhu@zju.edu.cn

endometrial epithelial cells require further investigation. Given the pivotal role of the SDF-1/CXCR4 axis in BMSC homing, we hypothesized that ATI-2341—a functionally selective allosteric modulator of CXCR4—could enhance the therapeutic efficacy of BMSCs in a rat model of IUA by optimizing their functional status. ATI-2341 trifluoroacetate (ATI-2341 TFA) was used in this study to pretreat BMSCs prior to transplantation. The aim of this study was to evaluate the effects of ATI-2341 TFA-pretreated BMSCs on endometrial thickness, cell proliferation, the balance of matrix metalloproteinase-9 (MMP-9) and tissue inhibitor of metalloproteinase-1 (TIMP-1) and the expression of epithelial markers in a rat IUA model. These investigations aim to provide preliminary insights into the role of CXCR4 signaling in BMSC-mediated endometrial repair.

MATERIALS AND METHODS

Reagents and instruments

Reagents: Trypsin (0.25%, containing EDTA, Cat. No. T1300, Beijing Solarbio Science & Technology Co., Ltd.); PBS buffer (pH 7.4, Cat. No. P1020, Beijing Solarbio Science & Technology Co., Ltd.); PVDF membrane (0.45 μm, Cat. No. IPVH00010, Merck Millipore); RIPA lysis buffer (containing PMSF, Cat. No. R0010, Beijing Solarbio Science & Technology Co., Ltd.); ATI-2341 TFA (purity > 98%, Cat. No. HY-107595, MCE), Chemical Structure ID: 121513892, a selective allosteric modulator of CXCR4; MTT assay kit (Cat. No. M1020, Beijing Solarbio Science & Technology Co., Ltd.); Sodium pentobarbital (Cat. No. P3761, Merck Sigma). The chemical structure of ATI-2341 TFA is shown in fig. 1.

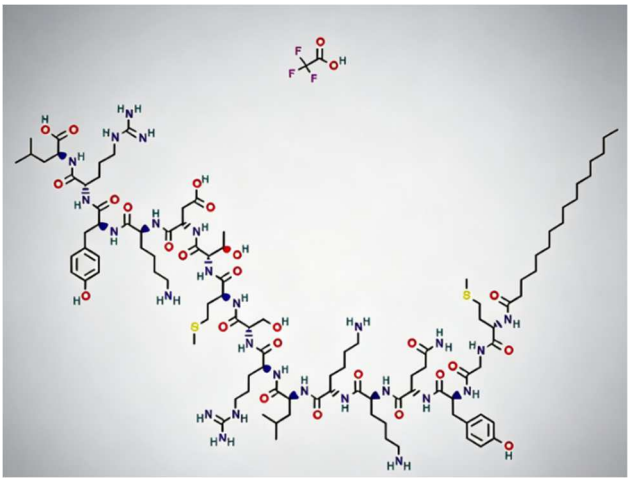

Fig. 1: Chemical structure of ATI-2341 TFA.

Instruments

Low-temperature high-speed centrifuge (Model: 5810R, Eppendorf, Germany); CO_2 cell culture incubator (Model: 3111, Thermo Fisher, USA); Microplate reader (Model: Multiskan FC, Thermo Fisher, USA); Electrophoresis and transfer system (Model: Mini-PROTEAN Tetra, Bio-Rad, USA).

Animal model

This study was approved by the Animal Ethics Committee of Women's Hospital, Zhejiang University School of Medicine (Approval No. 202510131) and all animal procedures were performed in accordance with the Guide for the Care and Use of Laboratory Animals. A completed ARRIVE checklist is provided as Supplementary Material.

A total of 50 female Sprague-Dawley (SD) rats, aged 5 weeks and weighing 100 ± 10 g, were purchased from Zhejiang University School of Medicine Laboratory Animal Research Center [License No. 20250325]. Surgeries were performed after one week of acclimatization feeding. Sample size was determined a priori using G*Power 3.1 software based on pilot experiment data (endometrial thickness: 185.4 ± 58.2 μm in model group vs. 298.6 ± 60.1 μ m in BMSCs+ATI-2341 TFA group). Setting $\alpha = 0.05$ and power = 0.80, a minimum of 7 rats per group was required. Considering an anticipated 20-25% modeling failure rate, 10 rats per group were included.

Anesthesia method

After weighing, the rats were intraperitoneally injected with 1% sodium pentobarbital (40 mg/kg) to induce anesthesia. The absence of the toe pinch reflex confirmed satisfactory anesthesia.

The surgical procedure was based on the reference literature (Xi *et al*., 2023) and modified: After 30 rats (5-week-old, 100 g) were anesthetized, an incision was made in the upper bladder. After the uterus was removed, both ends were clamped with vascular clips. The uterus was gently straightened using smooth forceps, and sterile gauze was wrapped around it to prevent extravasation. Normal saline (8 mL) was injected onto the surface of the uterus. A needle was then inserted into the uterine cavity and advanced approximately 3 cm. After puncture, excess normal saline was removed, followed by hot water injection. Finally, the uterus was repositioned. The abdominal cavity was flushed and the subcutaneous tissue and abdominal skin were sutured. Rats were injected with 2 mL of gentamicin 3 days after the operation.

Model validation

On the 7th day post-modeling, two model rats were randomly selected, euthanized, and uterine tissue samples were collected for hematoxylin and eosin (HE) staining. The successful establishment of the IUA model was histologically confirmed by reduced endometrial glands, disruption of epithelial cell continuity, and stromal fibrous tissue proliferation. The remaining rats were included in subsequent experimental groupings.

The pre-determined exclusion criteria include intraoperative death, uterine perforation, severe postoperative infection, or failure to meet the IUA histological criteria on the 7th day. Fifty initial rats were excluded without randomization.

Cultivation of BMSCs

Isolation and culture of BMSCs were performed according to the method of Soleimani and Nadri (2009). Rats were euthanized and the femurs and tibias were isolated after disinfection with 75% ethanol for 30 min. After flushing the samples with PBS, the bone marrow cavity was flushed with D-MEM until the cavity appeared white. The bone marrow suspension was centrifuged at 1 000 × g for 5 min, the supernatant was discarded and the pellet was resuspended and seeded in DMEM medium (1×10^6 cells/mL) for static culture in a 37ºC, 5% CO_2 saturated humidity incubator. The medium was refreshed every 2 days.

When the cells reached 90% confluence, they were passaged. The medium was removed after warming and trypsinization at 37ºC. The cells were washed twice with PBS and trypsin was added again for 30 seconds until the cells gradually became round under the microscope. The cells were repeatedly pipetted until no adherent cells remained, then centrifuged at 1 000 × g for 5 min. The supernatant was discarded and 2 mL of red blood cell lysis buffer (Cat. No. R1010, Beijing Solarbio) was added. The mixture was allowed to stand at room temperature for 5 min, centrifuged again (1 000 × g, 5 min) and the supernatant was discarded. For passaging, when the cells reached 90% confluence, 1 mL of 0.25% trypsin-EDTA (Cat. No. T1300, Beijing Solarbio) was added and digestion was performed at 37ºC for 1.5 min. After observing that the cells had rounded under the microscope, 2 mL of DMEM containing 10% FBS was immediately added to terminate digestion. A single-cell suspension was prepared by pipetting and the cells were subcultured at a 1:3 ratio.

Drug pretreatment: The third-generation BMSCs were taken for subsequent experiments. BMSCs + ATI-2341 TFA group: Add complete medium containing 100 ng/mL ATI-2341 TFA (dissolved in PBS containing 0.1% DMSO) and culture for 24 hours; Solvent control group (BMSCs +PBS) : Add an equal volume of PBS containing 0.1% DMSO and the culture conditions are the same as above; BMSCs group: Cultured in conventional complete medium for 24 hours. After pretreatment was completed, the cells were washed twice with PBS, collected by trypsin digestion, and resuspended in PBS to a final concentration of 1×10^6 cells/mL, ready for animal transplantation.

Identification of osteogenic and adipogenic differentiation

Experiments were conducted based on previous literature (Pittenger *et al*., 1999). Cells were fixed with 70% ethanol, washed with hydrogen peroxide, and stained with Alizarin Red solution for 30 minutes. After staining, they were washed with H_2O_2 and observed under a microscope.

After rat BMSCs were induced for 2 weeks, they were washed with PBS and fixed and stained with oil red solution. Upon washing with PBS, BMSCs were detected.

Western blot analysis

Following the method of Towbin *et al*. (1979), cells from each group were collected and lysed on ice for 30 min using RIPA lysis buffer (containing PMSF). The lysate was centrifuged at 12 000 × g for 15 min at 4ºC and the supernatant was collected. Protein concentration was determined using the BCA method. Protein samples were mixed with 5× loading buffer at a 4:1 ratio and boiled at 100 ℃ for 10 min. A total of 30 μg of protein per lane was separated by 10% SDS-PAGE and transferred to a PVDF membrane using the wet transfer method (300 mA, 90 min). The membrane was blocked with 5% non-fat milk at room temperature for 1 h. Primary antibody incubation: Rabbit anti-rat MMP-9 monoclonal antibody (1:1000, Cat. No. ab76003, Abcam), rabbit anti-rat TIMP-1 monoclonal antibody (1:1000, Cat. No. ab109125, Abcam) and mouse anti-rat GAPDH monoclonal antibody (1:5000, Cat. No. 60004-1-Ig, Proteintech) were incubated with the membrane on a shaker overnight at 4ºC.

The next day, the membrane was washed three times with TBST for 10 min each, followed by incubation with HRP-conjugated secondary antibodies (goat anti-rabbit IgG, 1:5000, Cat. No. SA00001-2, Proteintech; goat anti-mouse IgG, 1:5000, Cat. No. SA00001-1, Proteintech) at room temperature for 1.5 h. After three additional washes with TBST (10 min each), protein bands were visualized using the ECL chemiluminescent method. Grayscale values were analyzed using ImageJ software. The relative expression level of the target protein was calculated as the grayscale value of the target protein divided by the grayscale value of the internal reference GAPDH. Each experimental group was repeated independently three times.

Grouping

After model validation on day 7, 50 eligible rats were randomly assigned to 5 groups (n=10 each) by an independent researcher using a web-based random number generator (www.random.org): IUA model rats without any intervention. BMSCs group: IUA model rats injected via the tail vein with untreated BMSCs (1×10^6 cells/rat, dissolved in 0.5 mL PBS). BMSCs + ATI-2341 TFA group: IUA model rats injected via the tail vein with BMSCs pretreated with 100 ng/mL ATI-2341 TFA for 24 h (1×10^6 cells/rat, dissolved in 0.5 mL PBS). BMSCs + vehicle control group (BMSCs + PBS): IUA model rats injected via the tail vein with BMSCs pretreated with an equal volume of PBS (containing 0.1% DMSO) for 24 h (1×10^6 cells/rat,

dissolved in 0.5 mL PBS). Positive control group: IUA model rats intraperitoneally injected with estradiol valerate (0.2 mg/kg, once daily for 7 consecutive days). Group allocation was concealed in opaque envelopes and revealed immediately before treatment administration.

The concentration of 100 ng/mL used in this study was based on preliminary experimental results from our research group (concentration gradient screening: 0, 10, 50, 100 and 200 ng/mL) and literature reports (Rosenberger *et al*., 2024). At this concentration, no cytotoxicity was observed in the BMSC culture system (CCK-8 viability > 95%) and it effectively upregulated downstream CXCR4 signaling (p-ERK1/2 expression increased by 1.8-fold).

Detection of cell proliferation activity

The MTT assay was performed according to the method of Mosmann (1983). After 2 days of culture, BMSCs from each group were seeded into 96-well plates at a density of 5×10^3 cells per well in 200 μL of culture medium, with five replicate wells per group. After incubation for 24, 48, and 72 h, respectively, 20 μL of MTT solution (5 mg/mL) was added to each well, and the plates were incubated for an additional 4 h. The supernatant was then discarded and 150 μL of DMSO was added to each well. The plates were shaken for 10 min to dissolve the formazan crystals fully. The absorbance (OD) was measured at 490 nm using a microplate reader.

Immunohistochemistry

Rat uterine tissue samples were collected, fixed in paraformaldehyde, embedded in paraffin and sectioned. Endometrial thickness was examined microscopically after hematoxylin and eosin (HE) staining. Following deparaffinization and rehydration, sections were subjected to microwave antigen retrieval in citrate buffer (pH 6.0) for 15 min. Endogenous peroxidase activity was blocked by incubation with 3% H_2O_2 for 10 min at room temperature. Sections were then incubated with 50 μL of primary antibodies: rabbit anti-human broad-spectrum cytokeratin antibody (1:200 dilution, Cat. No. Z0622, Lot No. 200456, Dako) and mouse anti-rat vimentin antibody (1:400 dilution, Cat. No. M0725, Lot No. 190876, Dako) overnight (14-16 h) at 4ºC in a humidified chamber. After three washes with PBS, biotinylated goat anti-rabbit/mouse secondary antibody (1:200, Cat. No. E0432, Dako) was applied and incubated for 30 min at room temperature.

Following another PBS wash, streptavidin-horseradish peroxidase (1:200, Cat. No. K0679, Dako) was applied and incubated for 30 min at room temperature. Diaminobenzidine (DAB) chromogen solution (Cat. No. K3468, Dako) was applied for 3-5 min in the dark; color development was monitored microscopically and stopped by rinsing with running water. Sections were counterstained with hematoxylin for 30 s, dehydrated through a graded alcohol series, cleared in xylene and mounted with neutral balsam. The procedure was performed according to the method of Ramos-Vara (2005). Positive controls: Normal rat endometrial tissue was used as a positive control for cytokeratin and rat spleen tissue was used as a positive control for vimentin. Negative controls were prepared by substituting the primary antibody with PBS. Cytokeratin staining was evaluated as negative, weakly positive, positive, or strongly positive, corresponding to positive cell percentages of <5%, 5%-25%, 25%-50% and ≥75%, respectively. Vimentin staining was evaluated as negative, weakly positive, positive, or strongly positive, corresponding to positive cell percentages of 0%, <10%, 11%-50% and 50%-80%, respectively; >80% positive cells were also considered strongly positive. Two pathologists independently assessed immunohistochemical staining results under double-blind conditions. In cases of discrepant interpretations, a consensus was reached through discussion. Inter-observer agreement was evaluated using the Kappa test, with a Kappa value > 0.80.

Postoperative care and welfare

Postoperative analgesia was provided with buprenorphine (0.05 mg/kg, s.c., q12h for 3 days). Gentamicin (2 mg/kg, i.m., once daily for 3 days) was administered for infection prevention. Welfare assessments were performed every 6 h for the first 3 days and daily thereafter, monitoring body weight, posture, behavior, and wound healing. Predefined humane endpoints included >20% body weight loss, inability to eat/drink for >48 h, severe infection, or a pain score ≥3 (modified Rat Grimace Scale); no animals reached these endpoints. At experiment termination (day 7 post-treatment), euthanasia was performed by sodium pentobarbital overdose (150 mg/kg, i.p.), confirmed by cessation of heartbeat and respiration.

Blinding

Blinding was applied as follows: group allocation was concealed from the investigator performing tail vein injections; histopathological and immunohistochemical assessments were conducted by two pathologists blinded to group allocation; Western blot densitometry was performed by a researcher unaware of group assignment. *In-vitro* cell culture and data analysis were not blinded due to the nature of the interventions.

Statistical analysis

The primary outcome measure was endometrial thickness assessed by HE staining. Secondary outcome measures included BMSC proliferation (MTT assay), MMP-9 and TIMP-1 protein expression (Western blot), and cytokeratin/vimentin expression (immunohistochemistry). Data were analyzed with SPSS 22.0 statistical software, presented in GraphPad Prism 7, and reported as mean ± standard deviation.

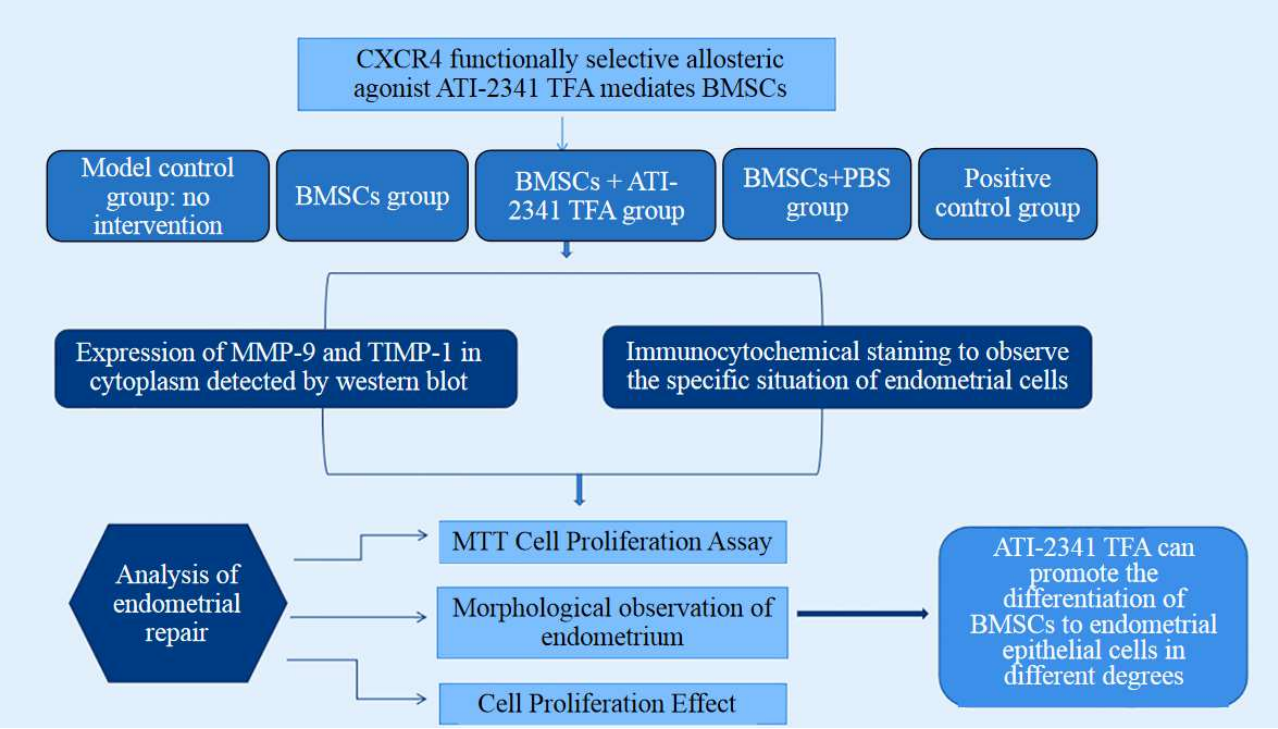

Fig. 2: Schematic diagram of research idea

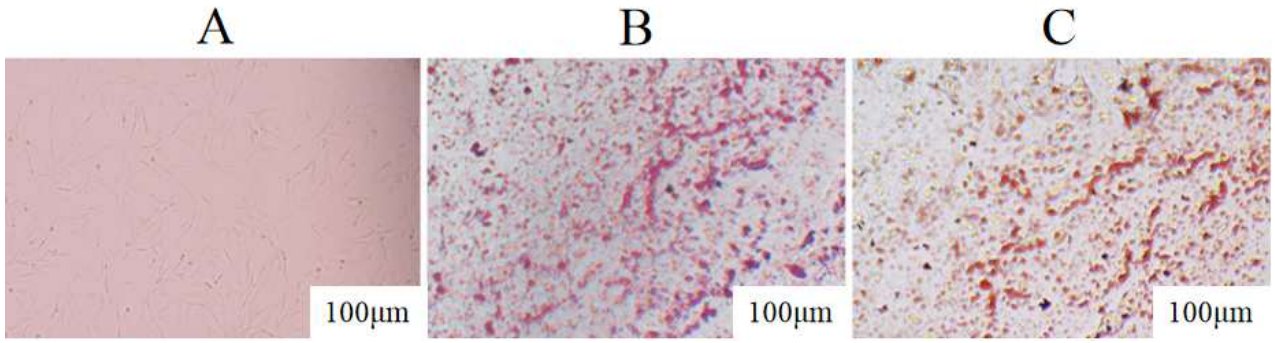

Fig. 3: Morphology of BMSCs
(A): Representative imaging of BMSCs at passage 3. (×400); (B): Representative imaging of BMSCs after osteogenic induction (×200); (C): Representative imaging of BMSCs after adipogenic induction (×400).

Comparisons between two groups were performed using an independent samples t-test. Comparisons across multiple time points were conducted using repeated measures analysis of variance (ANOVA), followed by post hoc pairwise comparisons using the Bonferroni method. A P value < 0.05 was considered statistically significant. No missing data occurred in this study. Outliers were defined using the Tukey method (values below Q1 - 1.5×IQR or above Q3 + 1.5×IQR). No outliers were detected or excluded from the final analysis. All analyses were performed on the complete dataset.

RESULTS

The morphology and differentiation ability of BMSCs

The technological roadmap is shown in fig. 2. After extraction of BMSCs, BMSCs at passage 3 were presented in long fusiform with different sizes and nuclei were observed; after osteogenic induction, dark red nodules appeared in the BMSCs, indicating osteogenic differentiation potential; in addition, through the induction of adipogenesis, red lipid droplets were observed in the cells, which indicates the adipogenic differentiation (Fig. 3).

The effect of ATI-2341 TFA on the protein expressions of MMP-9 and TIMP-1 in BMSCs

Western blot results showed that compared with the Model control group (1.00 ± 0.00), the relative protein expression levels of MMP-9 in both the BMSCs+ATI-2341 TFA group (0.35 ± 0.04) and the Positive control group (0.47 ± 0.03) were significantly decreased ($P < 0.05$).

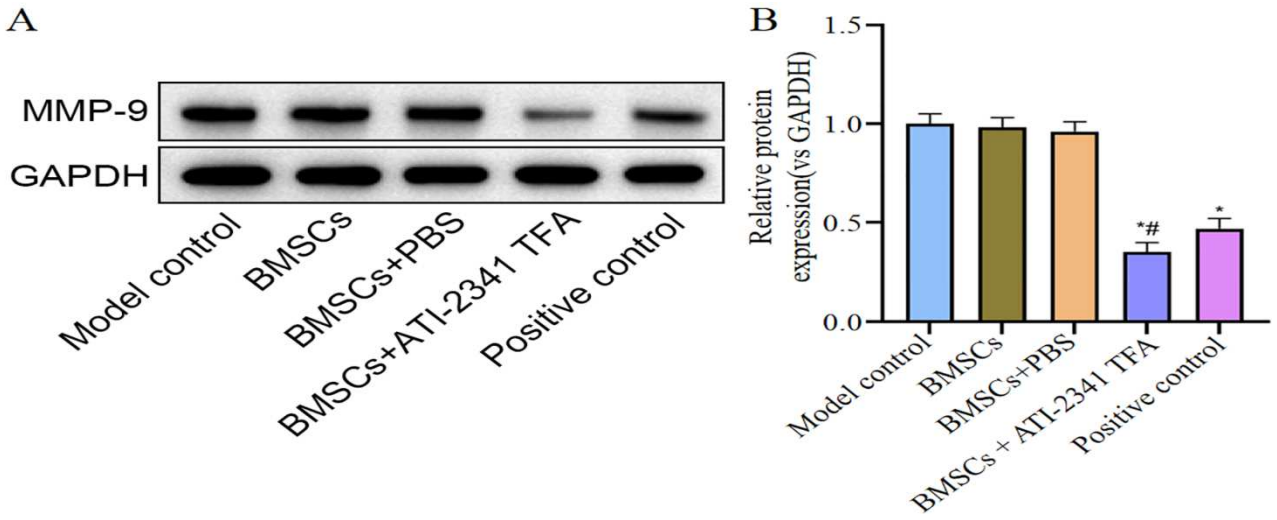

Fig. 4: The relative expression level of MMP-9 protein
(A) Representative Western blot bands; (B) Quantitative analysis of gray values. The relative expression level of MMP-9 is expressed as the ratio of MMP-9 to GAPDH. The data is mean ± SD, with n=3. *P < 0.05 vs. the Model control group; #P < 0.05 vs. Positive control group.

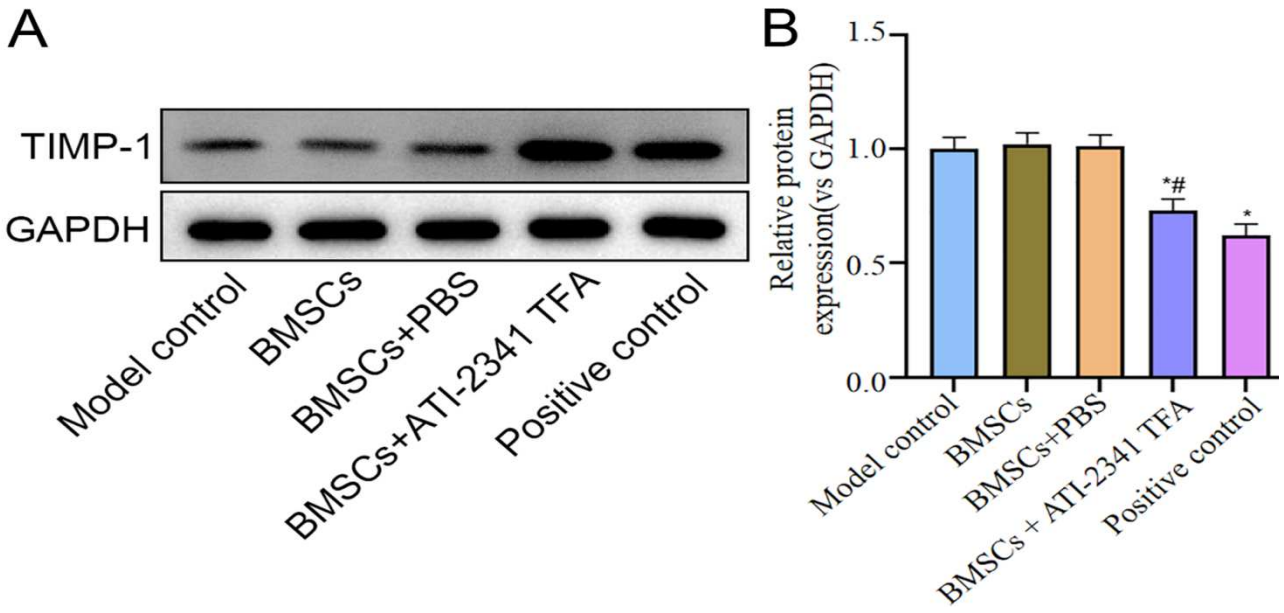

Fig. 5: Relative expression level of TIMP-1 protein
(A) Representative Western blot bands; (B) Quantitative analysis of gray values. The relative expression level of TIMP-1 is expressed as the ratio of TIMP-1 to GAPDH. The data is mean ± SD, with n=3. *P < 0.05 vs. the Model control group; #P < 0.05 vs. Positive control group.

Furthermore, the MMP-9 level in the BMSCs+ATI-2341 TFA group was significantly lower than that in the Positive control group ($P < 0.05$). There were no statistically significant differences in MMP-9 expression between the BMSCs group (0.98 ± 0.05) or the BMSCs+PBS group (0.96 ± 0.04) and the Model control group ($P > 0.05$). See Fig. 4.

Regarding the relative expression level of the TIMP-1 protein, compared with the Model control group (1.00 ± 0.00), it was significantly increased in both the BMSCs+ATI-2341 TFA group (0.73 ± 0.03) and the Positive control group (0.62 ± 0.04) ($P < 0.05$). Moreover, the TIMP-1 level in the BMSCs+ATI-2341 TFA group was significantly higher than that in the Positive control group ($P < 0.05$). There were no statistically significant differences in TIMP-1 expression between the BMSCs group (1.02 ± 0.05) or the BMSCs+PBS group (1.01 ± 0.03) and the Model control group ($P > 0.05$). See Fig. 5.

Table 1: Comparison of metabolic activities of BMSCs in each group (OD value, x±s).

Group	N	24 h	48 h	72 h
Model control group	10	0.112 ± 0.002	0.114 ± 0.019	0.115 ± 0.020
BMSCs group	10	0.112 ± 0.004	0.117 ± 0.018	0.118 ± 0.021
BMSCs+PBS group	10	0.111± 0.005	0.116 ± 0.020	0.117 ± 0.019
BMSCs + ATI-2341 TFA group	10	0.111± 0.006	0.131 ± 0.012*#	0.136 ± 0.019*#
Positive control group	10	0.112 ± 0.003	0.126 ± 0.024*	0.129 ± 0.016*
F		0.021	4.123	5.897
P		0.999	0.008	0.002

Note: Compared with the Model control group, *$P < 0.05$; Compared with the Positive control group, #$P < 0.05$.

Table 2: Comparison of endometrium thickness in each group (x±s).

Group	Quantity	Endometrial thickness (μm)
Model control group	10	187.36 ± 58.64
BMSCs group	10	202.45 ± 60.23
BMSCs+PBS group	10	198.76 ± 58.92
BMSCs + ATI-2341 TFA group	10	294.21 ± 59.97*#
Positive control group	10	258.82 ± 61.04*
F		5.234
P		0.001

Note: Compared with the Model control group, *$P < 0.05$; Compared with the Positive control group, #$P < 0.05$.

The effect of ATI-2341 TFA on the proliferation of BMSCs

The MTT assay results showed (Table 1) that at 24 h post-intervention, there was no statistically significant difference in OD values among the groups ($P > 0.05$). At 48 h and 72 h post-intervention, cell viability in the BMSCs+ATI-2341 TFA group was significantly higher than that in the BMSCs group and the BMSCs+PBS group ($P < 0.05$).

The cell viability rate in the Positive control group was also higher than that in the BMSCs group ($P < 0.05$) but was lower than that in the BMSCs+ATI-2341 TFA group ($P < 0.05$). There were no statistically significant differences between the BMSCs group and the BMSCs+PBS group at any time point ($P > 0.05$).

ATI-2341 TFA causes increased endometrial thickness

HE staining results showed (Table 2) that the endometrial thickness in the BMSCs+ATI-2341 TFA group (294.21 ± 59.97 μm) was significantly greater than that in the Model control group (187.36 ± 58.64 μm) ($P < 0.05$) and the Positive control group (258.82 ± 61.04 μm) ($P < 0.05$). The endometrial thickness in the Positive control group was also significantly greater than that in the Model control group ($P < 0.05$). There were no statistically significant differences in endometrial thickness between the BMSCs group (202.45 ± 60.23 μm) or the BMSCs+PBS group (198.76 ± 58.92 μm) and the Model control group ($P > 0.05$); however, both were significantly less than that in the BMSCs+ATI-2341 TFA group ($P < 0.05$).

Protein expression in the endometrium cytoplasm

The immunohistochemical staining results showed (Fig. 6) that in the BMSCs+ATI-2341 TFA group, endometrial glandular epithelial cells showed strong positive expression of keratin (cytoplasm brownish-yellow) and negative expression of vimentin (cytoplasm blue-purple). Positive control group Keratin positive expression (cytoplasm brownish-yellow), vimentin negative expression (cytoplasm blue-purple); Model control group Keratin negative expression (no obvious brownish-yellow color in the cytoplasm), vimentin positive expression (blue nucleus, brownish-yellow cytoplasm).

DISCUSSION

This study found that transplantation of BMSCs pretreated with ATI-2341 TFA into a rat model of IUA significantly increased endometrial thickness. This was accompanied by a decrease in the MMP-9/TIMP-1 ratio, upregulation of cytokeratin expression, and downregulation of vimentin expression. These results suggest that allosteric modulation targeting CXCR4 can optimize the reparative capacity of BMSCs within the damaged endometrial microenvironment. However, the specific mechanisms of action and the potential for clinical translation remain under cautionary interpretation.

We observed that following the transplantation of BMSCs pretreated with ATI-2341 TFA, the rat endometrial tissue exhibited strong positivity for cytokeratin and negativity for vimentin. Cytokeratin, as a marker of the epithelial cell cytoskeleton, is typically interpreted as indicating that cells have acquired an epithelial-like phenotype (Alsharif *et al*., 2021). However, this phenomenon has multiple possible biological explanations. One possibility is that ATI-2341 TFA directly induces the directed differentiation of BMSCs into endometrial epithelial cells.

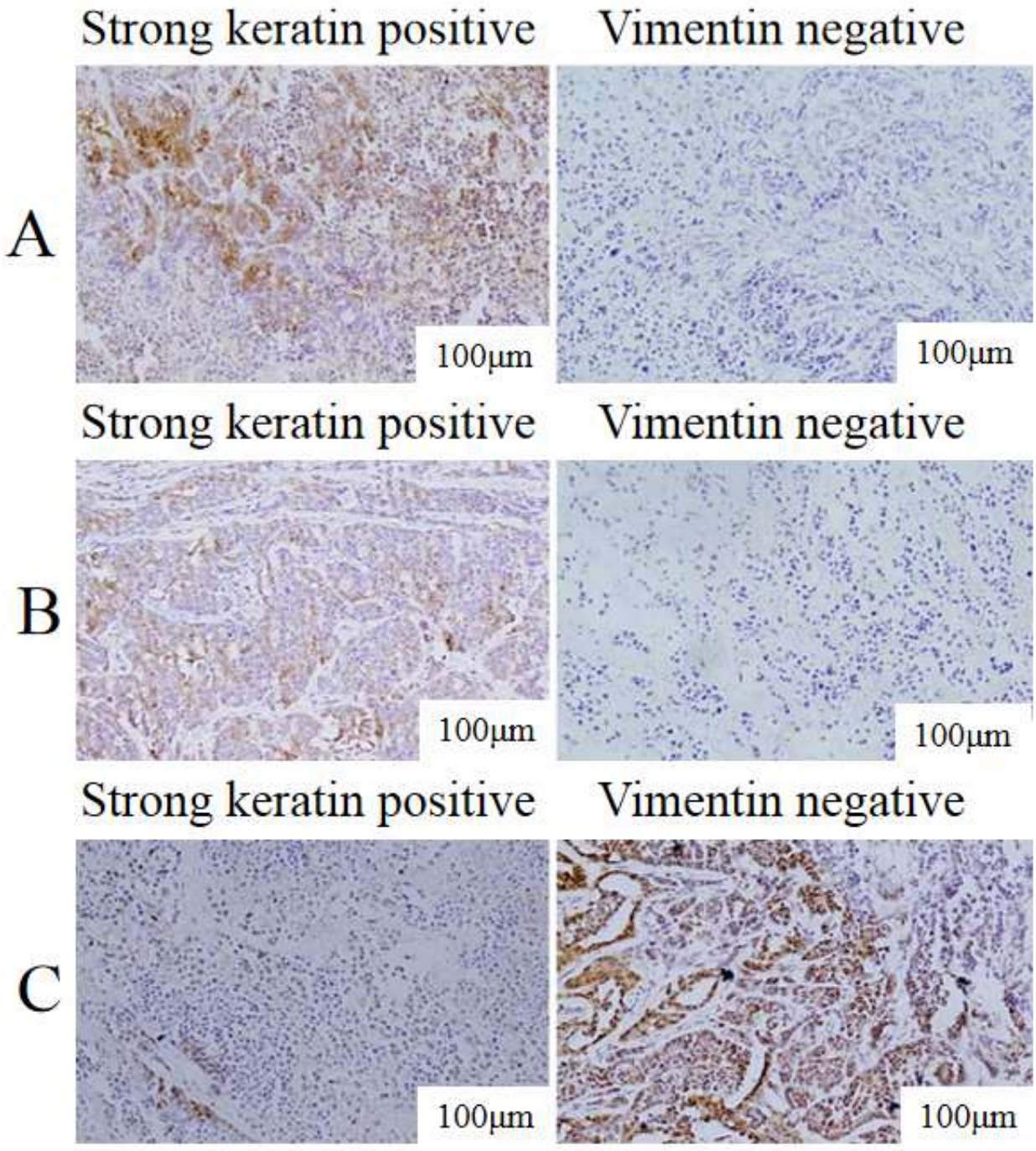

Fig. 6: Morphology of rat endometrial cells.
(A): BMSCs + ATI-2341 TFA group (×200); (B): Positive control group (×200); (C): Model control group (×200).

Although this hypothesis is attractive, the data from the current study are insufficient to support such a strong conclusion. The expression of epithelial markers does not equate to the formation of functional epithelial cells. Recent studies have shown that BMSCs can transiently express epithelial cell markers through a mechanism of "cellular plasticity" in specific inflammatory or injured microenvironments, but this does not necessarily imply lineage-directed differentiation or the formation of epithelial cells with functional characteristics such as polarity and tight junctions (Liu *et al*., 2024). Furthermore, ATI-2341 TFA, by enhancing CXCR4 signaling, may improve BMSC responsiveness to the injured microenvironment, enabling more effective homing to the injury site (Liu *et al*., 2022). Subsequently, through paracrine effects, they could modulate the residual phenotype of local cells, such as epithelial cells and fibroblasts, thereby indirectly contributing to the observed

expression of epithelial markers (Wang *et al*., 2024). The experimental design of this study cannot distinguish between the direct differentiation of BMSCs and their paracrine regulatory effects. Therefore, we interpret the current observations as indicating that BMSCs pretreated with ATI-2341 TFA acquire an "epithelial-like immunophenotype" within the endometrial microenvironment, rather than demonstrating that they "differentiate into functional endometrial epithelial cells." Future research needs to combine lineage-tracing techniques, functional epithelial characteristic assays, and single-cell transcriptomic analysis to definitively delineate the regulatory role of ATI-2341 TFA in lineage commitment of BMSCs.

The MMP-9/TIMP-1 balance is a key indicator of extracellular matrix (ECM) metabolism and fibrosis (Short *et al*., 2021). In this study, treatment with ATI-2341 TFA significantly decreased MMP-9 and increased TIMP-1. This pattern is typically associated with inhibiting excessive ECM degradation and promoting matrix stabilization, which, in theory, would be beneficial for alleviating endometrial fibrosis. This finding is consistent with the study by Han *et al*. (2025), which confirmed that BMSC implantation can improve the repair of damaged endometrium by modulating matrix remodeling. Notably, the magnitude of the modulation of the MMP-9/TIMP-1 balance by ATI-2341 TFA was significantly greater than that by estrogen. This difference suggests that ATI-2341 TFA may act directly on the CXCR4 receptor on the BMSC surface, activating downstream signaling pathways such as ERK1/2 and Akt. This, in turn, could alter their paracrine profile, leading to increased secretion of anti-fibrotic factors such as HGF and IL-10, and decreased secretion of pro-fibrotic factors such as TGF-β1 (De Souza *et al*., 2023). Concurrently, ATI-2341 TFA may enhance the recruitment of BMSCs to the injury site, allowing more BMSCs to exert local regulatory effects (Ferrini *et al*., 2021). However, this study did not directly assess the in vivo distribution and survival of the transplanted BMSCs, nor did it analyze their paracrine factor profile. Therefore, these hypothesized mechanisms require further experimental validation.

Although this study provides preliminary positive evidence, it is necessary to acknowledge its multiple limitations: first, insufficient mechanistic validation. We used the allosteric CXCR4 modulator ATI-2341 TFA, but did not perform functional rescue experiments using specific antagonists. Therefore, we cannot directly prove that the observed effects are mediated through the CXCR4 receptor. The potential off-target effects of ATI-2341 also need to be ruled out in future studies. Second, limitations of the cell proliferation assay. This study used the MTT assay to measure cellular metabolic activity as an indirect indicator of proliferation. Although commonly used, this method does not directly measure DNA synthesis or cell division. Future studies should incorporate more direct proliferation assays, such as EdU incorporation assays or Ki67 immunofluorescence staining, to confirm the promoting effect of ATI-2341 TFA on BMSC proliferation. Third, limited observation endpoints. This study only observed short-term histological changes and did not address long-term prognosis. Are there any tumorigenic risks associated with BMSC transplantation? What is their long-term survival and distribution in vivo? These safety issues have not been assessed.

Furthermore, whether histological improvements ultimately translate into functional improvements such as embryo implantation rates or fertility restoration remains unknown—fourth, translational limitations of the animal model. Although the rat IUA model used in this study is widely adopted, rodent endometrial physiology differs significantly from that of humans. The repair mechanisms, cycle regulation and responses to drugs may not be fully extrapolated to humans. Validation in animal models closer to humans, such as rabbits or pigs, is necessary before considering clinical translation.

CONCLUSION

In summary, this study demonstrates that BMSCs pretreated with ATI-2341 TFA can promote endometrial morphological repair in a rat model of IUA. This effect is associated with improved MMP-9/TIMP-1 balance and the acquisition of an epithelial-like phenotype by BMSCs. However, these findings should be considered preliminary and correlative, rather than establishing a definitive mechanism of action by which ATI-2341 induces directed differentiation of BMSCs via CXCR4. Future research should be systematically advanced along three dimensions: in-depth mechanistic studies (such as lineage tracing and CXCR4 blockade), assessment of functional endpoints (such as fertility evaluation), and translational feasibility (including safety studies and large-animal models). This comprehensive approach is necessary to fully evaluate the potential of targeting CXCR4 signaling to optimize stem cell therapy.

Acknowledgments
Not applicable.

Authors' contributions
Linhua Zhu: Conceptualization, Investigation, Formal analysis, Writing – original draft. Yongfang Yue and Lili Cao: Conceptualization, Supervision, Funding acquisition, Writing – review & editing.

Funding
This research received no specific grant from any funding agency in the public, commercial, or not-for-profit sectors.

Data availability statement
The datasets generated during and/or analysed during the current study are available from the corresponding author on reasonable request.

Ethical approval

This study was approved by the Animal Ethics Committee of Women's Hospital, Zhejiang University School of Medicine (Approval No. 202510131), and all animal procedures were performed in accordance with the Guide for the Care and Use of Laboratory Animals. This study was performed in adherence with the ARRIVE guidelines. See supplementary file for the ARRIVE checklist.

Conflict of interest

The authors declare that they have no conflict of interest.

Supplementary data

https://pjps.pk/uploads/2026/09/SUP1788772961.pdf

REFERENCES

Alsharif S, Sharma P, Bursch K, Milliken R, Lam V, Fallatah A, Phan T, Collins M, Dohlman P, Tiufekchiev S, Nehmetallah G, Raub CB and Chung BM (2021). Keratin 19 maintains E-cadherin localization at the cell surface and stabilizes cell-cell adhesion of MCF7 cells. *Cell Adh Migr*., **15**(1): 1–17.

Chen Y, Wang S, Chen X, Wu Z, He F and Chen Q (2025). Unraveling the mechanisms of bone diseases: Targeting dendritic cells in osteoimmunology for internal homeostasis balance. *Bone Res*., **13**(1): 81.

Cheng J, Zhang S, Gui Q, Pu Z, Chen Z, Wei Q, Qi H and Zhang J (2025). Identifying fibroblast-derived sFRP2 as a therapeutic target and engineering siRNA therapy for uterine scarring. *Nat Commun*., **16**(1): 6850.

De Souza IC, Takejima AL, Simeoni RB, Gamba LK, Ribeiro VST, Foltz KM, de Noronha L, de Almeida MB, Neto JRF, de Carvalho KAT, da Silveira PCL, Pinho R A, Francisco JC and Guarita-Souza LC (2023). Acellular biomaterials associated with autologous bone marrow-derived mononuclear stem cells improve wound healing through paracrine effects. *Biomedicines*., **11**(4): 1003.

Ferrini E, Stellari FF, Franceschi V, Macchi F, Russo L, Murgia A, Grisendi G, Villetti G, Dominici M and Donofrio G (2021). Persistency of mesenchymal stromal/stem cells in lungs. *Front Cell Dev Biol*., **9**: 709225.

Gonzalez-Meljem JM, Ivins S andoniadou CL, Le Tissier P, Scambler P and Martinez-Barbera JP (2023). An expression and function analysis of the CXCR4/SDF-1 signalling axis during pituitary gland development. *PLoS One*., **18**(2): e0280001.

Han R, Zhou H, Liang X, He S, Sun X, Guan Y and Song Y (2025). Thermo-sensitive ε-polylysine-heparin-poloxamer hydrogel-encapsulated BMSCs promote endometrial regeneration. *Mater Today Bio*., **31**: 101580.

Hu X, Wu H, Yong X, Wang Y, Yang S, Fan D, Xiao Y, Che L, Shi K, Li K, Xiong C, Zhu H and Qian Z (2023). Cyclical endometrial repair and regeneration: Molecular mechanisms, diseases and therapeutic interventions. *MedComm*., **4**(6): e425.

Jia Z, Wei Y, Zhang Y, Song K and Yuan J (2024). Metabolic reprogramming and heterogeneity during the decidualization process of endometrial stromal cells. *Cell Commun Signal*., **22**(1): 385.

Kim HK, Suh EJ, Cho S, Choi YS, Kim S and Park JH (2025). Derivation of granulosa-like cells from human endometrial iPSCs for autologous estradiol production. *Tissue Eng Regen Med*., **22**(8): 1199–1210.

Liu J, Gao J, Lu P, Wang Y, Xing S, Yan Y, Han R, Hao P and Li X (2024). Mesenchymal stem cell-derived exosomes as drug carriers for delivering miRNA-29b to ameliorate inflammation in corneal injury via activating autophagy. *Invest Ophthalmol Vis Sci*., **65**(6): 16.

Liu Y, Liu N, Li X, Luo Z and Zhang J (2022). Ginsenoside Rb1 modulates the migration of bone-derived mesenchymal stem cells through the SDF-1/CXCR4 axis and PI3K/Akt pathway. *Dis Markers*., **2022**: 5196682.

Ma M, Wang S, Wang K, Jiang B, Li J and Hou S (2025). CXCL12 links bladder cancer and diabetes as a potential biomarker. *Sci Rep*., **15**(1): 19017.

Mosmann T (1983). Rapid colorimetric assay for cellular growth and survival: Application to proliferation and cytotoxicity assays. *J Immunol Methods*., **65**(1-2): 55-63.

Park A, Kim SE, Yu J, Son D, Kim KS, Koh E and Park KS (2024). Cadherin-6 is a novel mediator for the migration of mesenchymal stem cells to glioblastoma cells in response to stromal cell-derived factor-1. *FEBS Open Bio*., **14**(7): 1192–1204.

Pittenger MF, Mackay AM, Beck SC, Jaiswal RK, Douglas R, Mosca JD, Moorman MA, Simonetti DW, Craig S and Marshak DR (1999). Multilineage potential of adult human mesenchymal stem cells. *Science*., **284**(5411): 143-147.

Qin Z, Yu Q and Long Y (2025). Unveiling the pathological landscape of intrauterine adhesion: Mechanistic insights and exosome-biomaterial therapeutic innovations. *Int J Nanomedicine*., **20**: 9667–9694.

Ramos-Vara JA (2005). Technical aspects of immunohistochemistry. *Vet Pathol*., **42**(4): 405-26.

Rosenberger T, Bell AM, Reifferscheid G, Smith KEC, Schäffer A, Ternes TA and Buchinger S (2024). Extrapolation of cytotoxic masked effects in planar in vitro assays. *Anal Bioanal Chem*., **416**(15): 3519–3532.

Short CS, Quinlan RA, Wang X, Preda VG, Smith A, Marchesi JR, Lee YS, MacIntyre DA, Bennett PR and Taylor GP (2021). Vaginal microbiota, genital inflammation and extracellular matrix remodelling collagenase: MMP-9 in pregnant women With HIV, a potential preterm birth mechanism warranting further exploration. *Front Cell Infect Microbiol*., **11**: 750103.

Soleimani M and Nadri S (2009). A protocol for isolation and culture of mesenchymal stem cells from mouse bone marrow. *Nat Protoc*., **4**(1): 102-6.

Song YT, Liu PC, Tan J, Zou CY, Li QJ, Li-Ling J and Xie HQ (2021). Stem cell-based therapy for ameliorating

intrauterine adhesion and endometrium injury. *Stem Cell Res Ther*., **12**(1): 556.

Towbin H, Staehelin T and Gordon J (1979). Electrophoretic transfer of proteins from polyacrylamide gels to nitrocellulose sheets: Procedure and some applications. *Proc Natl Acad Sci USA*., **76**(9): 4350-4.

Wang YH, Zhao CZ, Wang RY, Du QX, Liu JY and Pan J (2022). The crosstalk between macrophages and bone marrow mesenchymal stem cells in bone healing. *Stem Cell Res Ther*., **13**(1): 511.

Wang F, Dai H, Zhou Z, Shan Y, Yu M, Sun J, Sheng L, Huang L, Meng X, You Y and Sheng M (2024). Astragalus polysaccharides augment BMSC homing via SDF-1/CXCR4 modulation: A novel approach to counteract peritoneal mesenchymal transformation and fibrosis. *BMC Complement Med Ther*., **24**(1): 204.

Xi J, Pan Y, Jin C, Liu J, Cheng J and Xu B (2023). Evaluation of different rat models intrauterine adhesion models and improvement of the technique for their establishment. *Exp Anim*., **72**(2): 274–284.

Yang R, Shen H, Wang M, Zhao Y, Zhu S, Jiang H, Li Y, Pu G, Chen X, Chen P, Lu Q, Ma J and Zhang Q (2024). Expression of SDF-1/CXCR4 and related inflammatory factors in sodium fluoride-treated hepatocytes. *PLoS One*., **19**(6): e0302530.

Yuan L, Cao J, Hu M, Xu D, Li Y, Zhao S, Yuan J, Zhang H, Huang Y, Jin H, Chen M and Liu D (2022). Bone marrow mesenchymal stem cells combined with estrogen synergistically promote endometrial regeneration and reverse EMT via Wnt/β-catenin signaling pathway. *Reprod Biol Endocrinol*., **20**(1): 121.

Zhang X, Zhang S and Wang T (2022). How the mechanical microenvironment of stem cell growth affects their differentiation: A review. *Stem Cell Res Ther*., **13**(1): 415.

Zhao Y, Xu A, Liu D, Liu N, Li Y, Yao Z, Tian F, Tang H and Li Y (2023). An endometrium of type C along with an endometrial thickness of < 8 mm are risk factors for ectopic pregnancy after stimulated cycles with fresh embryo transfer. *BMC Pregnancy Childbirth*., **23**(1): 713.